

Experimental implementation of low-cost and robust sensorless control based on SOGI-FLL estimator for electric vehicles

Riad Bouzidi¹, Ismail Ghadbane¹, Mohammed Boukhari¹, Ahmed Bendib¹, Abdelhammid Kherbachi²

¹Department of Electrical Engineering, Electrical Engineering Laboratory, M'Sila University, M'Sila, Algeria

²Renewable Energy Development Center, Algiers, Algeria

Article Info

Article history:

Received Apr 10, 2022

Revised Aug 1, 2022

Accepted Aug 16, 2022

Keywords:

dSPACE micro labox

Electric vehicle

Induction motor

Second-order generalized
integrator-frequency-locked
loop

Sensorless control

ABSTRACT

Sensorless control techniques of electric motor dedicated to electric vehicles (EVs) offer low-cost and high operating performance. In this paper, a low-cost and robust speed-sensorless control scheme based on a second-order generalized integrator-frequency-locked loop method (SOGI-FLL) is proposed with only one current sensor. The SOGI-FLL is introduced to estimate accurately the motor angular speed from a measured current signal. While the scalar control technique, based on a single loop speed regulation, is used to determine the control signals. According to the proposed control scheme, the overall system will be very effective in terms of low-cost control and easy practical implementation, which have a great impact on electric vehicle applications. dSPACE micro labox platform is used to implement the proposed control scheme to drive an induction motor. The obtained results confirm the effectiveness and high performance of the proposed control to properly estimate the angular speed and drive the induction motor.

This is an open access article under the [CC BY-SA](https://creativecommons.org/licenses/by-sa/4.0/) license.



Corresponding Author:

Ismail Ghadbane

Department of Electrical Engineering, Electrical Engineering Laboratory, M'sila University

Route Ichebilia, Boîte Postale 166 M'sila, M'sila, 28000, Algeria

Email: ismail.ghadbane@univ-msila.dz

NOMENCLATURE

F_{ad}	Aerodynamic drag force	A	Vehicle acceleration
P	Air density	J_m	Moment of inertia of the rotor of the motor
C_d	Drag coefficient	G	Gear ratio
A	Surface of the vehicle	R_ω	Wheel radius
V	Velocity	η_G	Gear efficiency
F_{rr}	Rolling resistance force	T_L	Load torque in the motor
K_r	Tire rolling resistance coefficient	W_M	Motor speed
m	Total mass of the vehicle	K_f	Friction coefficient
g	Acceleration of gravity	J_T	Total inertia
F_{hc}	Hill climbing resistance	EV	Electric vehicle
A	Road slope angle	IM	Induction motor
F_a	Acceleration force		

1. INTRODUCTION

The majority of industrial workers in the electric vehicles field, strive to obtain powerful comfortable vehicles that are capable of covering long distances in a safe manner. However, these features and characteristics in vehicles require highly complicated and expensive electrical control systems, as well as an increase in vehicle size, which leads to a lack of demand. To this end, researchers in this field have been interested to establish a compromise solution between the two parts (manufacturers and consumers) by designing simple and low-cost electric drive systems while keeping the electric vehicle's strength and comfort, as well as being able to travel long distances [1]–[5].

Electric vehicles depend on different electric drive systems according to the type of the used electric motor such as DC motor, synchronous or asynchronous AC motor, and the permanent magnet synchronous motor (PMSM) [6]. Besides, the selection of an electric motor drive for electric vehicles depends on the conditions of its specifications. Some of them require a high speed, so they need a moving system that depends on a fast motor, such as a motor with a variable impedance switched reluctance motor (SRM). Others require a large torque, so they need a moving system with a high torque accelerator such as the PMSM. Further, there is a specification that requires large speeds and torques, so it must have a suitable system, like the one that depends on the brushless DC motors (BLDC) motor [7], [8].

Despite asynchronous motors' simplicity and power, as well as their low price, global demand for their drive system in the field of electric vehicles is continually decreasing. This effect is due to the fact that this type of drive system produces a vehicle with medium speed and torque compared to other drive systems. In this regard, during the last three decades, there has been a lot of research focused on designing and enhancing driving systems based on induction motors intended for electric vehicles, making them rival to many current driving systems that rely on strong motors such as SRM, BLDC, and PMSM. Such a drive system, as mentioned before, can provide very fast and powerful electric vehicles [9]. The present research, on one hand, addresses the development of electrical drive system devices and improving their efficiency. On the other hand, it focuses on developing and improving control algorithms for the elements of the drive system (inverter, rectifier, motor).

The presence of a speed sensor in the stirring system of an induction motor makes it more accurate and powerful. However, due to the high cost of the sensor and its very sensitive structure (the weakest element in the stirring loop), in addition to making the stirring system more complex, many researchers have thought about getting rid of it and replacing it with an estimator or a speed monitor based on a mathematical algorithm. Among the presented ideas, Bolognani *et al.* [10] have proposed a very simple open-loop method to estimate the angular speed by using the mathematical model of the rotor part of an IM four-parameters equivalent circuit in the α - β frame. This method has a significant drawback which is the lack of speed correction due to the continuous increase of the error between the estimated speed and the real speed. To overcome the drawback of this method, several works that focus on estimating the motor speed using the closed-loop estimation strategy have been presented. For instance, [11] Luenberger observer, [12] lower-ranked observer, and [13] sliding mode observer have been suggested to estimate motor angular speed. Although the obtained results are significantly better than the open-loop estimation method, the sensitivity of these methods to the change of the motor's parameters due to the dependence on the induction motor model, such as the stator resistance R_s , is an issue.

To deal with this issue, the [14]–[16] has proposed a model reference adaptive system (MRAS) based speed observer for induction motor drive. This method has provided good results through its dependence on an adaptive mechanism that takes into account the change of motor parameters. With the emergence of artificial intelligence strategies, it, in turn, moved to speed monitors. Wlas *et al.* [17] have adopted a speed controller based on the artificial neural network (ANN), which has provided good results in the transitional and permanent system. However, since all the afore-mentioned closed-loop estimation methods depend on current and voltage measurements of the stator motor side, it may make the speed estimation subject to measurement noise. In [18]–[20] an extended Kalman filter is suggested as a solution to address this problem by taking into account the measurement noise. This adopted method has ensured a high accuracy of speed estimation. Nevertheless, the main disadvantages of this observer lie in its complex algorithm and the difficulty of selecting the two matrixes Q and R . The SOGI-FLL technique is another effective solution that has been applied for sensorless speed estimation (or flux estimation) [21]–[24]. For instance, Wanget *al.* [25] have proposed a speed-sensorless control that includes an improved SOGI-FLL-based-speed estimation for induction motor drives. The obtained results have revealed that the proposed technique has contributed to improving the accuracy of the speed estimation and reducing system complexity as well.

Generally speaking, all the stated methods require expensive current and voltage sensors (two sensors at least), and most of them, except the last methods, suffer from a lack of filtering algorithms. In this regard, a low-cost speed-sensorless control scheme based on the SOGI-FLL technique is proposed. This

control scheme is applied to drive a three-phase IM for an electric vehicle. The proposed control scheme is based on only one sensor for a single current measurement. In addition, the control signals of the converter are determined by using a scalar control based on a single loop speed regulation. Further, a SOGI-FLL-based estimation is adopted to detect with high precision the angular speed of the motor. Such an estimation based on SOGI-FLL which characterizes by its simplicity of implementation and high harmonics filtering capabilities can contribute to improving the speed estimation performance. All in all, the designed control scheme is very simple, low cost, and easy to implement in practice. Experimental results are presented to prove the effectiveness and robustness of the proposed control scheme for IM drive by using dSPACE micro labox.

2. DYNAMIC MODELING AND ANALYSIS OF EV

In order to study the control of an electric vehicle, it is necessary to have a mathematical model. The model of an electric vehicle is described by the dynamic of the vehicle from the tensile forces developed by its actuators and the forces of resistance to displacement, as presented in Figure 1. It is worth mentioning that the variables' nomenclature is provided in Appendix A.

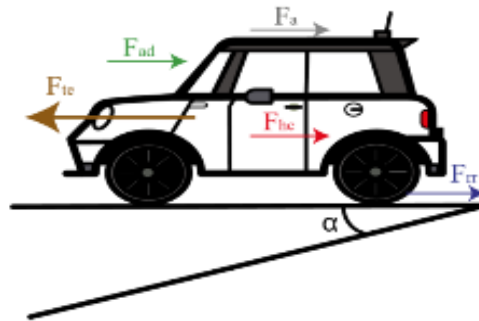


Figure 1. Forces acting on a vehicle

The aerodynamic drag force F_{ad} is the viscous resistance of air acting upon the vehicle, expressed by (1):

$$F_{ad} = \frac{1}{2} \rho C_d A V^2 \quad (1)$$

The rolling resistance force F_{rr} is produced by the tire flattening at the roadway contact surface, and it can be defined as (2).

$$F_{rr} = K_r m g \quad (2)$$

The hill-climbing resistance (F_{hc} with positive operational sign) and the downgrade force (F_{hc} with negative operational sign) are given by (3).

$$F_{hc} = \pm m G \sin(\alpha) \quad (3)$$

The acceleration force F_a can be obtained as (4).

$$F_a = F_{la} + F_{wa} \quad (4)$$

Where F_{la} is the force required to give a linear acceleration, and F_{wa} is the force required to give angular acceleration, which can be represented as:

$$F_{la} = m a \quad (5)$$

$$F_{wa} = J_m \frac{G^2}{\eta_G R_w^2} a \quad (6)$$

The total tractive effort F_{te} is given by:

$$F_{te} = F_{ad} + F_{rr} + F_{hc} + Fa \quad (7)$$

The load torque of the vehicle T_L can be defined by (8).

$$T_L = R_w F_{te} \quad (8)$$

The mechanical equation (in the motor referential) used to describe each wheel drive can be expressed by (9).

$$J_T \frac{dW_m}{dt} + K_f W_m + T_L = T_e \quad (9)$$

The electromagnetic torque T_e is given by (10).

$$T_L = \frac{T_L W}{G} = \frac{R_w F_{te}}{G} \quad (10)$$

3. PROPOSED SENSORLESS CONTROL

In the voltage/frequency control, the speed of the induction motor is controlled by the adjustable magnitude of the stator voltages and frequency in such a way that the air gap flux is always maintained at the desired value at the steady-state. Sometimes this scheme is called the scalar control because it focuses only on the steady-state [26]. It can be seen that at steady-state and in low slip regions, the stator resistance drop is assumed to be zero according to the one phase equivalent circuit of an IM as shown in Figure 2. Therefore, the stator flux is directly controlled by the ratio of the phase voltage of the stator and the electric frequency ω_s as indicated by (11).

$$V_s = R_s I_s + \frac{d\varphi_s}{dt} \approx j\omega_s \varphi_s \quad (11)$$

In order to keep the stator flux φ_s constant, the ratio of $\frac{V_s}{f}$ would also be constant at different speeds. In this case, the relation between the frequency and the amplitude of the stator voltage is linear and it can be defined as (12).

$$\frac{V_s}{f_s} = 2\pi\varphi_s = Const \quad (12)$$

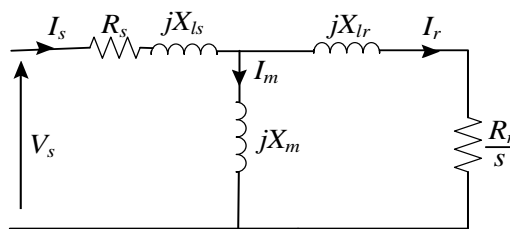


Figure 2. The equivalent electrical circuit of an IM

On the other hand, the magnetizing current I_m , which is necessary to establish the air-gap flux, and the load current I_r , which is a function of the working point and the applied load, make up the stator current I_s . The equivalent resistance $\frac{R_r}{s}$ represents the influence of load and rotor resistance. The entire leakage reactance in the rotor and the rotor resistance, respectively, are represented by X_{lr} and R_r , and X_{ls} is the leakage reactance in the stator. The electromagnetic torque transmitted to the rotor can be expressed as:

$$T_{em} = 3p \frac{R_r V_s^2}{s\omega_s \left(\left(\frac{R_r}{s} \right)^2 + X_{lr}^2 \right)} \quad (13)$$

$$T_{em} = 3 \frac{p}{R_r} \varphi_s^2 s \omega_s \quad (14)$$

where p is the number of poles pair and s is the slip.

The electromagnetic torque is solely dependent on the slip speed if the stator flux is kept constant, implying that its variation as a function of the slip is almost linear. Again, to keep φ_s constant, the ratio of $\frac{V_s}{f_s}$ would be constant at different speeds. As the speed increases, the stator voltages must, therefore, be proportionally increased in order to keep a constant ratio of $\frac{V_s}{f_s}$. However, because of the slip, the synchronous speed is not the real speed. The slip is relatively tiny at no-load torque and the speed ω_r is very close to the synchronous speed ω_s . As a result, the open-loop scalar control was unable to precisely control the speed in the presence of load torque. For this reason, a closed-loop controller with speed measurement is required for applications that need high-speed accuracy and quick responses to either load torque or speed reference variation [26]. The mechanical dynamics of the IM can be expressed as (15).

$$T_{em} - K_f \omega_r - T_r = \frac{J}{p} \frac{d\omega_r}{dt} \quad (15)$$

Where K_f is the viscosity coefficient. Taking the load torque T_L out of the equation, the transfer function of the rotor speed ω_r and the electromagnetic torque T_{em} , represented by a first-order system, as in (16).

$$\frac{\omega_r}{T_{em}} = \frac{1}{K_f + \frac{J}{p} s} \quad (16)$$

The structure of the proposed control scheme is shown in Figure 3. As seen, the SOGI FLL technique is introduced to estimate the operating frequency, f_s , of the stator single-phase current i_a ; measured through one current sensor. Accordingly, the rotor speed estimate, \hat{N}_r , of the motor is obtained by multiplying the estimated frequency f_s and the amount $\frac{60}{p}(1-s)$. The amount of the slip factor (s) is considered constant in our work. This assumption is valid in the case of scalar control since the motor speed is almost around the nominal value. The estimated speed, \hat{N}_r , is compared to its reference speed N_r^* provided by the vehicle model corresponding to the applied mechanical force M_f . The resulted error is, then, handled by a PI controller to get the slip speed reference, ω_{sl}^* . This slip speed is limited for stability and overcurrent prevention. By adding ω_{sl}^* to $\hat{\omega}_r$, the synchronous speed reference, ω_s^* , is then achieved. After that, the voltage reference V_s^* is obtained by using the scalar V/f control algorithm and the angular phase reference θ_s^* is achieved by integrating ω_s^* . These references, V_s^* and θ_s^* , are used to generate the inverter's signal commands (S_i) by means of a pulse width modulator (PWM).

It is worth mentioning, that the voltage reference V_s^* is achieved based on the constant Volts/Hertz (V/f) control method, which is defined as (17).

$$V_s^* = \begin{cases} \frac{(V_{s, rat} - V_{s, 0})}{f_{s, rat}} f_s + V_{s, 0} & ; \text{for } f_s < f_{s, rat} \\ V_{s, rat} & ; \text{for } f_s \geq f_{s, rat} \end{cases} \quad (17)$$

Where $V_{s, rat}$ and $V_{s, 0}$ are the rated value and the RMS value at zero frequency of the stator voltage, respectively and $f_{s, rat}$ is the stator rated frequency.

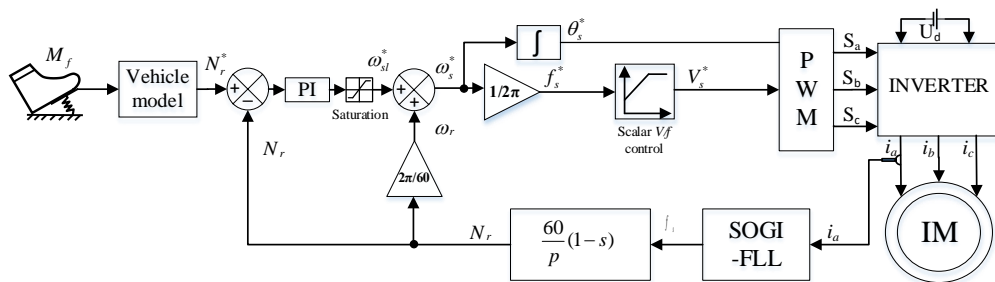


Figure 3. The proposed speed control scheme of an IM

4. SOGI-FLL METHOD

The SOGI-FLL is a simple adaptive filter applied for the parameter's estimation of a single-phase voltage such as; frequency, amplitude, orthogonal components, and phase angle. This method has the advantage of good harmonics filtering capabilities and low computation burdens. The block diagram of the SOGI-FLL is shown in Figure 4, which is composed of two main parts, the SOGI, and the FLL. The SOGI is a second-order filter that provides filtered in-phase and in-quadrature phase voltage components; v_α and v_β ; with respect to input voltage v_{in} . The FLL is in charge of estimating the angular frequency (ω) of the input voltage v_{in} that uses for the tuning of the SOGI filter.

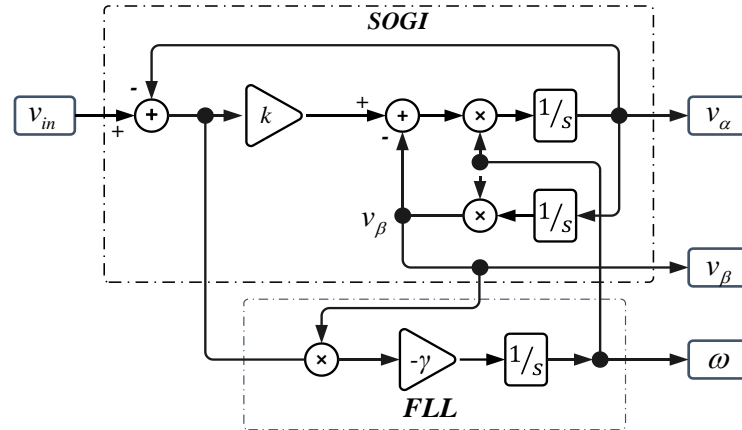


Figure 4. Block diagram of the SOGI-FLL scheme

The SOGI act as a band-pass filter (BPF) for v_α and a low-pass filter (LPF) for v_β , in which their expressions can be given as [27]-[28]:

$$v_\alpha(s) = \frac{k\omega s}{s^2 + k\omega s + \omega^2} v_{in}(s) \quad (18)$$

$$v_\beta(s) = \frac{ks}{s^2 + k\omega s + \omega^2} v_{in}(s) \quad (19)$$

Where k is the gain of the SOGI chosen as a trade-off between speed of dynamic response and harmonic filtering performance. On the other hand, the estimated frequency by the SOGI-FLL can be expressed as (20).

$$\omega = -\frac{\gamma}{s} (v_{in}(s) - v_\alpha(s)) v_\beta(s) \quad (20)$$

where γ is the FLL gain which can be defined as (21).

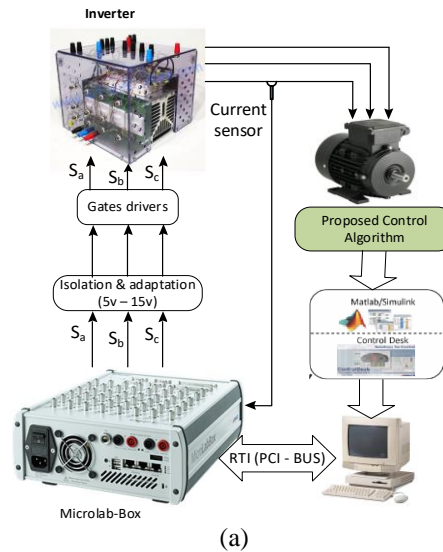
$$\gamma = \frac{k\omega_o}{V^2} \Gamma \quad (21)$$

Being V the estimated amplitude and Γ is a positive gain that depends on the settling time of the FLL.

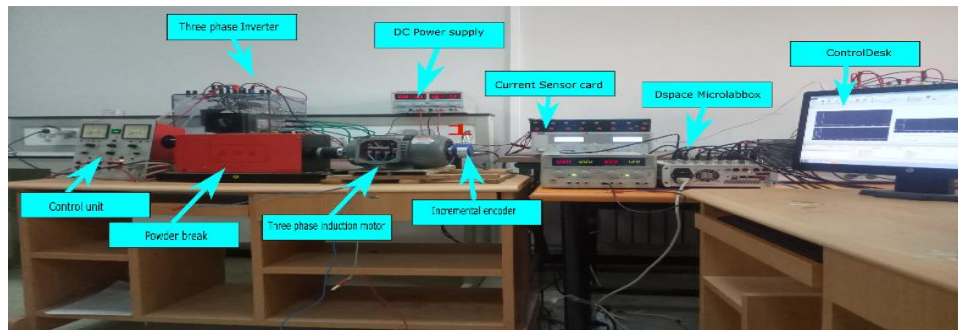
5. EXPERIMENTAL RESULTS

To assess the effectiveness of the proposed control scheme, a testbed is conducted based on dSPACE micro labox, as shown in Figure 5. Figure 5(a) depicts the block diagram of the implemented MATLAB/Simulink model based on the dSPACE micro labox. While Figure 5(b) displays the built testbed which consists of the following devices:

- Three-phase 0.55 kW induction motor with the parameters given $P_n=0.55$ kw, $V_n=230/400$ V, $i_n=2.48/1.43$ A, $N_n=1390$ rpm, $f=50$ Hz.
- dSPACE Micro Labox, Ds1102, with control desk software
- Powder brake with torque control unit
- Current sensor
- GW instek numerical Oscilloscope
- Semikron converter composed of IGBT three-phase inverter and rectifier
- Incremental encoder speed sensor DC 5V-24V 4096 P/R



(a)



(b)

Figure 5. Configuration of (a) the implemented Simulink model based on dSPACE and (b) the experimental setup

The proposed speed controller based on the SOGI-FLL estimator is tested versus speed variation at no-load and load change. Figure 6 shows the obtained results for speed reference changes in a range of 1000 r/min to 1300 r/min, at no-load. From Figure 6(a) which depicts the responses of estimated, measured, and reference speed, it can be observed that the estimated speed overlapped with the measured one, just with a tiny delay time when the speed reference changes. However, this delay does not affect the performance of the vehicle's speed as seen in the zoom as shown in Figure 6(b). In addition, it can be noticed that the proposed controller regulates the estimated speed to the reference speed with good transient response. According to Figures 6(c) to 6(d) which present the measured phase current, i_a , and its amplitude, it can be noticed that they follow the variation of the speed. Furthermore, the estimated frequency by the SOGI-FLL estimator, shown in Figure 6(e), also, follows the variation of the speed. In Figure 6(f) it is shown that the estimated phase angle remains almost unchanged even under speed variation. Figure 7 shows the performance of the proposed controller for speed reversal reference change, from 1200 to -1200 rpm, during no-load operation. As shown in Figure 7(a), with a modification in the structure of SOGI FLL by speed reference insertion, the estimated speed tracks the negative speed reference with an acceptable transient response as shown in Figure 7(b), meanwhile it is matched with the measured one. In addition, the phase current (i_a) and its amplitude shown in Figures 7(c) and 7(d), illustrate that the current varies when the speed change. Further, from the responses of the estimated frequency and phase provided in Figures 7(e) and 7(f), it can be noted that the frequency and phase almost remain constant, just a pulse occurs in the frequency response at the moment of speed variation.

In the third test, the electric vehicle is operating with a load of 1.5Nm at $t=20$ s, after a no-load operation start. The obtained results, presented in Figure 8 illustrate that the proposed speed controller is capable to keep the estimated EV speed at its reference when the load change as shown in Figures 8(a) and 8(b). In addition, it can be noticed that estimated and measured speeds are overlapped. From Figures 8(c) and 8(d), it can be observed that the current increases corresponding to load change. Further, as shown in Figures 8(e) and 8(f), the estimated frequency and phase almost remain unchanged even when a load is added.

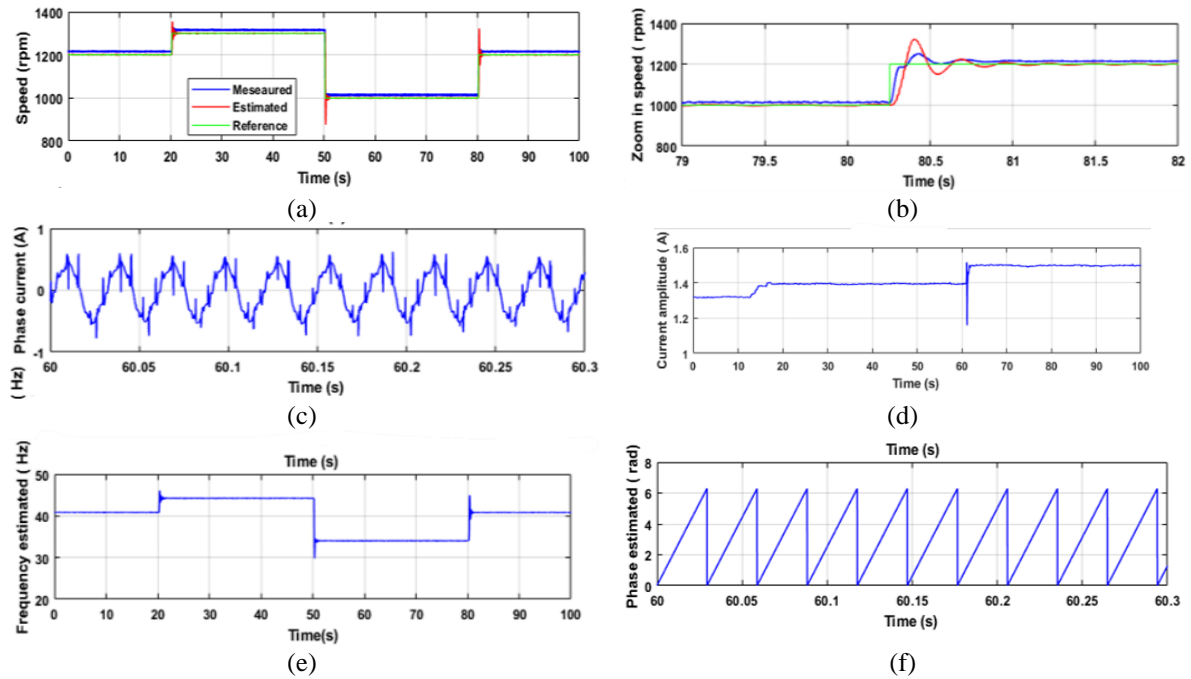


Figure 6. Experimental performance of SOGI-FLL estimator during (1300-1000 tr/min) speed change: (a) reference, estimated and measured speed, (b) zoom in speed 1000 rpm, (c) current phase a, (d) current amplitude, (e) estimated frequency, and (f) estimated phase

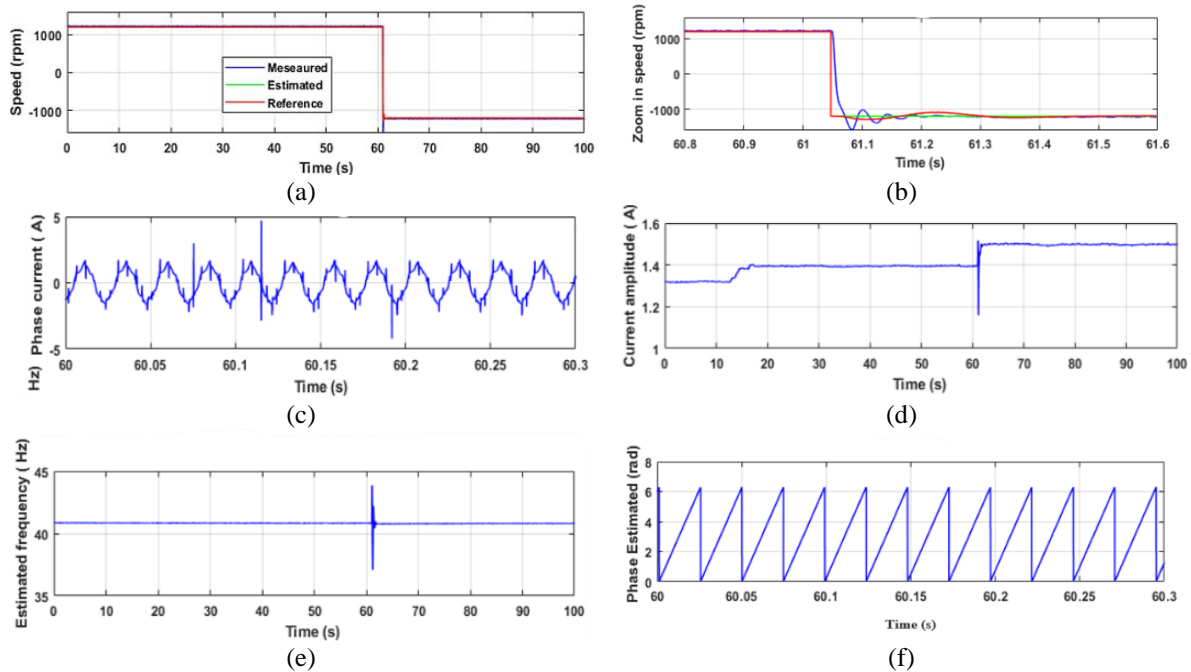


Figure 7. Experimental performance of SOGI-FLL estimator during reversal speed change: (a) reference, estimated and measured speed, (b) zoom in speed 1200 rpm, (c) current phase a, (d) current amplitude, (e) estimated frequency, and (f) estimated phase

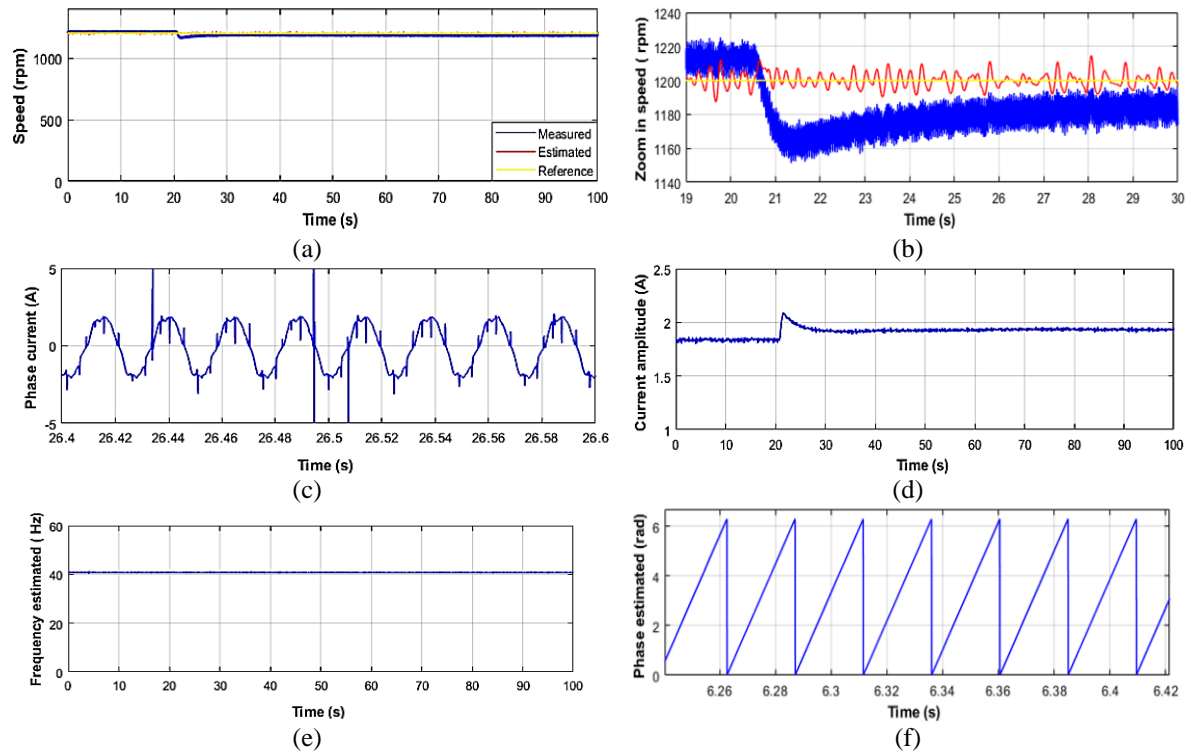


Figure 8. Experimental performance of SOGI-FLL estimator during load application: (a) reference, estimated and measured speed, (b) zoom in speed 1000 rpm, (c) current phase a, (d) current amplitude, (e) estimated frequency, and (f) estimated phase

In the last case, the electric vehicle operates with different loads. The load variation is performed by changing the slope of the road as described in Figure 9. The obtained results for this case are presented in Figure 10. According to Figure 10, the following observations for each step can be made.

- Step1: The electric motor of our vehicle model works with a 1Nm load (straight road), until $t=20s$. The estimated speed follows its desired reference (i.e., 1200 rpm), as depicted in Figure 10(a). Figures 10(c) and 10(d) illustrate that the phase current (i_a) and its amplitude are constants. While Figures 10(e) and 10(f) present that an appropriate estimation of the frequency and phase is achieved.
- Step 2: The load is between (1Nm and 2Nm), the estimated speed stay follows its new reference, and matches with the measured one. In Figures 10(c) and 10(d), the phase current and its amplitude increase as the load increases.
- Step 3: The applied load, here, is 2Nm, the estimated speed follows its rated reference with a slight change in the speed, which does not affect the performance of the electric vehicle. The current and its amplitude during this scenario remain constants in Figures 10(c) and 10(d).
- Step 4: In this step, a load of 1Nm is applied. The estimated speed quickly backs to its rated reference in Figure 10(a), while the phase current and its amplitude decrease when the load decreases as shown in Figure 10(b), Figures 10(c) and 10(d).

Note that the estimated frequency and phase; presented in Figures 10(e) and 10(f); almost remain unvaried during the load change. Consequently, the obtained results demonstrate that the proposed controller speed based on the SOGI-FLL estimator is strong to track the rotor speed throughout a large speed range and different load operating conditions.

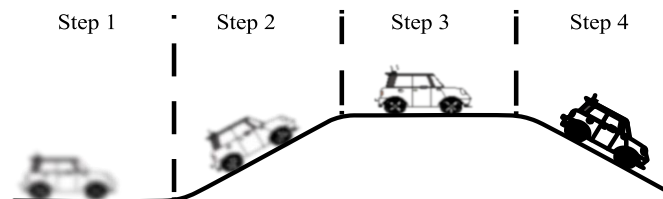


Figure 9. The slope of the road

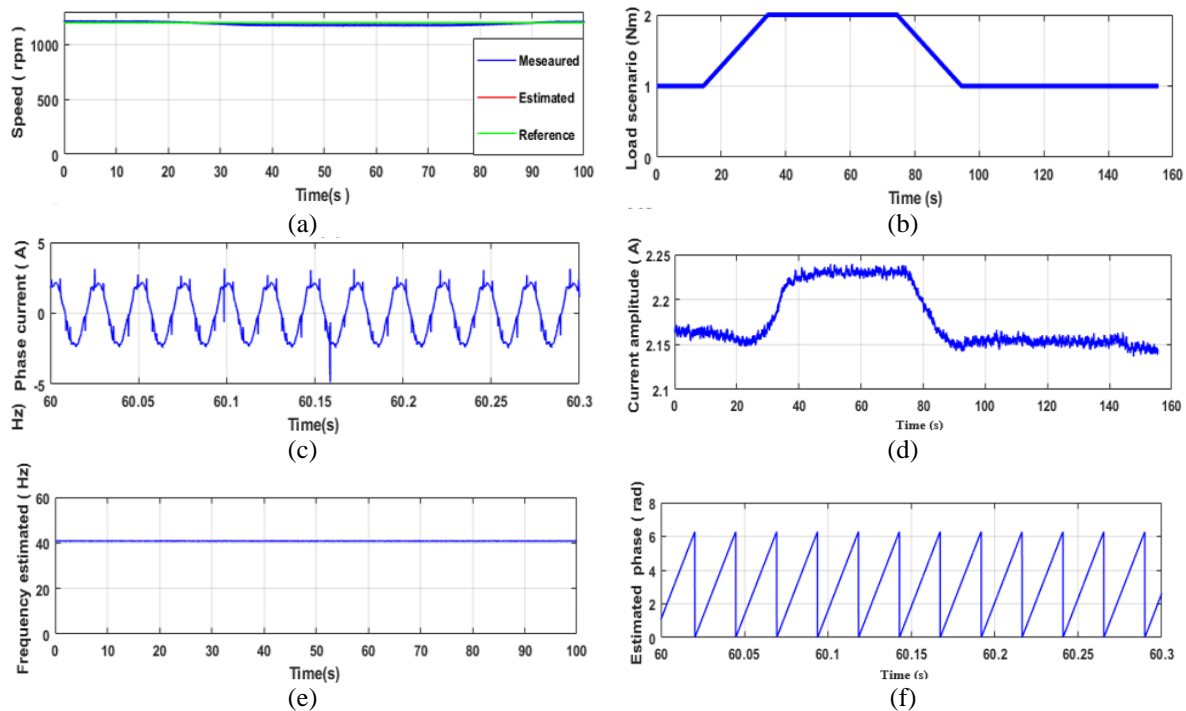


Figure 10. Experimental performance of SOGI-FLL estimator during load scenario application: (a) reference, estimated and measured speed, (b) load scenario, (c) current phase a, (d) current amplitude, (e) estimated frequency of the current phase i_a , and (f) estimated phase

6. CONCLUSION

In this research paper, a simple and robust speed-sensorless control scheme intended for IM-based electric vehicle driving was proposed. This control scheme is based on only a single current sensor with one angular speed regulation loop. In addition, the rotor speed information was determined through a frequency estimated by the SOGI-FLL method. The performance of the proposed SOGI-FLL estimator-based speed control scheme was tested experimentally based on dSPACE Micro Labbox and under speed reference changes. In addition, it was implemented to track a designed trajectory of an electric vehicle. The obtained results have demonstrated the effectiveness and the robustness of the proposed controller in achieving good responses under motor speed changes. In addition, they have confirmed its efficiency in tracking perfectly the desired electric vehicle trajectory. Moreover, a special test that considers the negative speed reference was carried out, in which a proposed method is suggested to deal with this test case since the SOGI estimator can't handle the negative frequency. The obtained results have shown the ability of the control approach to deal with such an operating condition.




REFERENCES

- [1] M. Ehsani, K. V. Singh, H. O. Bansal and R. T. Mehrjardi, "State of the art and trends in electric and hybrid electric vehicles," *Proceedings of the IEEE*, vol. 109, no. 6, pp. 967-984, 2021, doi: 10.1109/JPROC.2021.3072788.
- [2] C. C. Chan and Y. S. Wong, "The state of the art of electric vehicles technology," *The 4th International Power Electronics and Motion Control Conference, IPEMC*, vol. 1, pp. 46-57, 2004.
- [3] C. C. Chan, "The state of the art of electric and hybrid vehicles," *Proceedings of the IEEE*, vol. 90, no. 2, pp. 247-275, 2002, doi: 10.1109/5.989873.
- [4] L. Situ, "Electric Vehicle development: The past, present & future," *3rd International Conference on Power Electronics Systems and Applications (PESA)*, 2009, pp. 1-3.
- [5] E. I. Mbadiwe, E. Sulaiman, Z. Md. Ahmad, and M. F. Omar, "Permanent magnet flux switching motor technology as a solution for high torque clean electric vehicle drive," *International Journal of Power Electronics and Drive System*, vol. 10, no. 2, pp. 575-584, 2019, doi: 10.11591/ijpeds.v10.i2.pp575-584.
- [6] A. Havel, M. Sobek, L. Stepanec, and J. Strossa, "Optimization of permanent magnet parameters in axial flux rotary converter for HEV drive," *Energies*, vol. 15, no. 3, pp. 1-12, 2022, doi: 10.3390/en15030724.
- [7] C. C. Chan and K. T. Chau, "An overview of power electronics in electric vehicles," *IEEE Transactions on Industrial Electronics*, vol. 44, no. 1, pp. 3-13, 1997, doi: 10.1109/41.557493.
- [8] A. Emadi, Y. J. Lee and K. Rajashekara, "Power electronics and motor drives in electric, hybrid electric, and plug-in hybrid electric vehicles," *IEEE Transactions on Industrial Electronics*, vol. 55, no. 6, pp. 2237-2245, 2008, doi: 10.1109/TIE.2008.922768.




- [9] A. Haddoun, M. E. H. Benbouzid, D. Diallo, R. Abdessemed, J. Ghouili and K. Srairi, "A loss-minimization DTC scheme for EV induction motors," *IEEE Transactions on Vehicular Technology*, vol. 56, no. 1, pp. 81-88, 2007, doi: 10.1109/TVT.2006.889562.
- [10] S. Bolognani, L. Peretti and M. Zigliotto, "Parameter sensitivity analysis of an improved open-loop speed estimate for induction motor drives," *IEEE Transactions on Power Electronics*, vol. 23, no. 4, pp. 2127-2135, 2008, doi: 10.1109/TPEL.2008.925178.
- [11] T. S. Kuen, M. H. Shin and D. S. Hyun, "Speed sensorless stator flux-oriented control of induction motor in the field weakening region using Luenberger observer," *IEEE 34th Annual Conference on Power Electronics Specialist, PESC '03.*, 2003, pp. 1460-1464 vol.3, doi: 10.1109/PESC.2003.1216802.
- [12] M. Cirrincione, M. Pucci, G. Cirrincione and G. -A. Capolino, "Sensorless control of induction motors by reduced order observer with MCA EXIN + Based Adaptive Speed Estimation," *IEEE Transactions on Industrial Electronics*, vol. 54, no. 1, pp. 150-166, Feb. 2007, doi: 10.1109/TIE.2006.888776.
- [13] Zhang Yan, Changxi Jin and V. Utkin, "Sensorless sliding-mode control of induction motors," *IEEE Transactions on Industrial Electronics*, vol. 47, no. 6, pp. 1286-1297, Dec. 2000, doi: 10.1109/41.887957.
- [14] I. Benloulou, S. Drid, L. Chrifi-Alaoui and M. Ouriagli, "Implementation of a new MRAS speed sensorless vector control of induction machine," *IEEE Transactions on Energy Conversion*, vol. 30, no. 2, pp. 588-595, 2015, doi: 10.1109/TEC.2014.2366473.
- [15] E. Dehghan-Azad, S. Gadoue, D. Atkinson, H. Slater, P. Barrass and F. Blaabjerg, "Sensorless control of IM based on stator-voltage MRAS for limp-home EV applications," *IEEE Transactions on Power Electronics*, vol. 33, no. 3, pp. 1911-1921, 2018, doi: 10.1109/TPEL.2017.2695259.
- [16] M. Korzonek, G. Tarchala and T. Orlowska-Kowalska, "Simple stability enhancement method for stator current error-based MRAS-type speed estimator for induction motor," *IEEE Transactions on Industrial Electronics*, vol. 67, no. 7, pp. 5854-5866, 2020, doi: 10.1109/TIE.2019.2960726.
- [17] M. Wlas, Z. Krzeminski, J. Guzinski, H. Abu-Rub and H. A. Toliyat, "Artificial-neural-network-based sensorless nonlinear control of induction motors," *IEEE Transactions on Energy Conversion*, vol. 20, no. 3, pp. 520-528, 2005, doi: 10.1109/TEC.2005.847984.
- [18] M. L. Jayaramu, H. N. Suresh, M. S. Bhaskar, D. Almakhles, S. Padmanaban and U. Subramaniam, "Real-time implementation of extended Kalman filter observer with improved speed estimation for sensorless control," *IEEE Access*, vol. 9, pp. 50452-50465, 2021, doi: 10.1109/ACCESS.2021.3069676.
- [19] E. Zerdali and M. Barut, "The comparisons of optimized extended Kalman filters for speed-sensorless control of induction motors," *IEEE Transactions on Industrial Electronics*, vol. 64, no. 6, pp. 4340-4351, 2017, doi: 10.1109/TIE.2017.2674579.
- [20] M. Montanari, S. M. Peresada, C. Rossi and A. Tilli, "Speed sensorless control of induction motors based on a reduced-order adaptive observer," *IEEE Transactions on Control Systems Technology*, vol. 15, no. 6, pp. 1049-1064, 2007, doi: 10.1109/TCST.2007.899714.
- [21] H. Wang, Y. Yang, X. Ge, Y. Zuo, Y. Yue and S. Li, "PLL- and FLL -based speed estimation schemes for speed-sensorless control of induction motor drives: Review and New Attempts," *IEEE Transactions on Power Electronics*, vol. 37, no. 3, pp. 3334-3356, 2022, doi: 10.1109/TPEL.2021.3117697.
- [22] R. Zhao, Z. Xin, P. C. Loh and F. Blaabjerg, "A novel flux estimator based on multiple second-order generalized integrators and frequency-locked loop for induction motor drives," *IEEE Transactions on Power Electronics*, vol. 32, no. 8, pp. 6286-6296, 2017, doi: 10.1109/TPEL.2016.2620428.
- [23] Z. Xin, R. Zhao, F. Blaabjerg, L. Zhang and P. C. Loh, "An improved flux observer for field-oriented control of induction motors based on dual second-order generalized integrator frequency-locked loop," *IEEE Journal of Emerging and Selected Topics in Power Electronics*, vol. 5, no. 1, pp. 513-525, 2017, doi: 10.1109/JESTPE.2016.2623668.
- [24] H. Wang, Y. Yang, Y. Zuo, S. Li, X. Hu and X. Ge, "A speed estimation scheme based on an improved SOGI-FLL for speed-sensorless control of induction motor drives," *IECON 2020 The 46th Annual Conference of the IEEE Industrial Electronics Society*, 2020, pp. 852-857, doi: 10.1109/IECON43393.2020.9255253.
- [25] K. Lee and Y. Han, "Reactive-power-based robust MTPA control for v/f scalar-controlled induction motor drives," *IEEE Transactions on Industrial Electronics*, vol. 69, no. 1, pp. 169-178, 2022, doi: 10.1109/TIE.2021.3055183.
- [26] A. Bendib, A. Chouder, K. Kara, A. Kherbachi, S. Barkat and W. Issa, "New modeling approach of secondary control layer for autonomous single-phase microgrids," *Journal of the Franklin Institute*, vol. 356, no. 13, pp. 6847-6874, 2019, doi: 10.1016/j.jfranklin.2019.04.020.
- [27] C. A. Busada, S. Gomez Jorge, A. E. Leon and J. A. Solsona, "Current controller based on reduced order generalized integrators for distributed generation systems," *IEEE Transactions on Industrial Electronics*, vol. 59, no. 7, pp. 2898-2909, 2012, doi: 10.1109/TIE.2011.2167892.
- [28] S. Golestan, J. M. Guerrero, J. C. Vasquez, A. M. Abusorrah and Y. Al-Turki, "Modeling, tuning, and performance comparison of second-order-generalized-integrator-based FLLs," *IEEE Transactions on Power Electronics*, vol. 33, no. 12, pp. 10229-10239, 2018, doi: 10.1109/TPEL.2018.2808246.

BIOGRAPHIES OF AUTHORS






Riad Bouzidi    He received his Engineer degree in Electrotechnics and Magister degree in electrical engineering from Biskra University in 2006 and 2009, respectively. He received his Ph.D. in electrical engineering from Biskra University in 2019. Since 2013 he has held a teaching and research position in the Department of Electrical Engineering of M'sila University, Algeria. His research interests are in electrical drives, power electronics, and power systems. He can be contacted at: riad.bouzidi@univ-msila.dz.






Ismail Ghadbane    He received his Ph.D degree in electrical engineering in 2016 from Biskra University. His research interests are in electrical drives, power electronics, power energy quality, and intelligent control systems. Since 2013 he has held a teaching and research position in the Department of Electrical Engineering of M'SILA University, Algeria. He can be contacted at: ismail.ghadbane@univ-msila.dz.






Mohammed Boukhari    He was born in Bordj Bou Arreridj, Algeria, and he is a second-year doctoral student in renewable energy at the university of M'sila. His research interests include renewable energy and electric vehicle technology and control of motors. He can be contacted at: mohammed.boukhari@univ-msila.dz.



Ahmed Bendib    He was born in M'sila Village, Algeria, in 1987. He received an engineer degree in electronics, option control, and M.S. degree in control of electro-energetic systems from the University of M'sila, M'sila, Algeria, in 2010 and 2014, respectively, and a Ph.D. degree in Electronics from the University of Blida, Blida, Algeria, in 2021. From 2011 to 2012, he was an Assistant Professor in the Department of Electronics at the University of M'sila. He is the author of five articles. His research interests include modeling, simulation, and control of single-phase inverters-based Microgrid systems, STM32F Microcontroller-based control, and inverters for photovoltaic applications. He can be contacted at: ahmeddib28@gmail.com.



Abdelhamid Kherbachi    He was born in M'sila Village, Algeria, in 1986. He received an engineer degree in electronics, option control, and M.S. degree in control of electro-energetic systems from the University of M'sila, M'sila, Algeria, in 2010 and 2014, respectively, and a Ph.D. degree in Electronics from the University of Blida, Blida, Algeria, in 2021. From 2011 to 2013, he was an Assistant Professor in the Department of Electronics at the University of M'sila. From 2014 to 2018, he became an Assistant Professor with the Laboratory of Electronics at the University of M'sila. Since October 2020, he has been an Assistant Engineer with the department of wind energy division, Renewable Energy Development Center (CDER) in Alger, Algeria. He is the author of five articles. His research interests include the Development of inverter electronic cards, simulation, and control of single-phase power inverters within microgrids, STM32F Microcontroller-based control, and inverters for photovoltaic applications. He can be contacted at: a.kherbachi@cderr.dz and kherbachi.h@gmail.com.